INSTITUTE OF PHYSICS PUBLISHING and INTERNATIONAL ATOMIC ENERGY AGENCY NUCLEAR FUSION

Nucl. Fusion **46** (2006) S926–S932 doi:10.1088/0029-5515/46/10/S09

Fast ion loss in a 'sea-of-TAE'

E.D. Fredrickson[1], N.N. Gorelenkov[1], R.E. Bell[1], J.E. Menard[1], A.L. Roquemore[1], S. Kubota[2], N.A. Crocker[2] and W. Peebles[2]

[1] Princeton Plasma Physics Laboratory, Princeton, NJ, USA
[2] University of California, Los Angelos, CA, USA

Received 23 December 2005, accepted for publication 28 April 2006
Published 22 September 2006
Online at stacks.iop.org/NF/46/S926

Abstract
Super-thermal fast ions provide a source of free energy to excite instabilities, which in turn can enhance the loss of fast ions. It has been proposed that when multiple modes with resonances closely spaced in phase space reach sufficient amplitude so that the fast ion trajectories overlap, very rapid non-linear growth can occur. The modification of the fast ion distribution by this loss may in turn excite additional, otherwise stable, modes, leading to an 'avalanche' effect greatly enhancing the transport of fast ions (Berk H.L., Breizman B.N., Fitzpatrick J. and Wong H.V. 1995 *Nucl. Fusion* **35** 1661). It has been proposed that in ITER (ITER Physics Basis Editors *et al* 1999 *Nucl. Fusion* **39** 2137), the transport of fast ions will be through a similar interaction of many modes. In NSTX (Ono M. *et al* 2000 *Nucl. Fusion* **40** 557) bursts of multiple TAE-like instabilities are correlated with fast ion losses in a manner which qualitatively resembles avalanche behaviour.

PACS numbers: 52.55.Fa, 52.35.Bj, 52.50.Gj

1. Introduction

The International Tokamak Experimental Reactor (ITER) [1] will be heated primarily by the super-Alfvénic alpha particles from the D–T fusion reaction. These fast ions provide a potential source of free energy to excite instabilities such as toroidal alfvén eigenmodes (TAE) [2–4], which may then enhance fast ion transport and reduce the heating efficiency. The dynamics of the growth and saturation of these instabilities, particularly when multiple modes are present, is complex. A major focus of research on present machines is to provide benchmarks for models of mode growth, saturation and effect on transport.

The National Spherical Torus Experiment (NSTX) is a low aspect ratio ($R/a \approx 1.3$) tokamak [5]. The confining magnetic field is low (3–5 kG) so that the 60–90 kV neutral beam ions are super-Alfvénic. In typical operational regimes on NSTX the magneto-hydrodynamic (MHD) instability spectrum is dominated by modes driven by fast ions. Some of the fast ion instabilities are correlated with drops in the neutron rate, indicating fast ion losses.

2. Experimental results

The toroidal mode number, frequency and amplitude of fast ion driven instabilities are measured with arrays of Mirnov coils mounted inside the vacuum vessel and an array of three quadrature reflectometers [6]. The Mirnov coil arrays measure the toroidal mode number of the modes and provide an indirect measure of the mode amplitudes. However, interpretation of the amplitude data is dependent on the radial eigenfunction of the modes. The toroidal mode numbers are determined from the relative phase of the signals between the twelve coils which make up a toroidal array mounted on the vacuum vessel just below the outboard midplane.

The quadrature reflectometers operate at frequencies of 30 Ghz, 42 Ghz and 49.85 Ghz corresponding to plasma cut-off layer densities of approximately $1.1 \times 10^{13}\,\mathrm{cm}^{-3}$, $2.2 \times 10^{13}\,\mathrm{cm}^{-3}$ and $3.1 \times 10^{13}\,\mathrm{cm}^{-3}$, respectively. The reflectometers provide an internal measurement of the mode amplitude in terms of the radial displacement of the flux surface on the outboard midplane. As will be discussed below, the internal magnetic and electric field fluctuation amplitudes can be inferred from this measurement of displacement.

Data from one representative NSTX discharge will be shown. In this example the plasma is heated from 0.06 s with two neutral beam sources. The beam voltage has been reduced from a more typical 80 to 65 kV for both sources. The total injected neutral beam heating power is 2.1 MW. The plasma current is ramped until ≈0.26 s where it flattops at 800 kA. The toroidal field is ≈4.5 kG. The central electron temperature during the times of interest is ≈1.1 to 1.9 kV and the central density is ≈2.5 to $3.7 \times 10^{13}\,\mathrm{cm}^{-3}$. The target plasma is nominally Helium, although a substantial amount of deuterium is injected by the neutral beams and recycled from the vacuum vessel walls, limiters and divertor target plates. The helium inhibits the transition to H-mode; operating in L-mode keeps the density profile peaked allowing

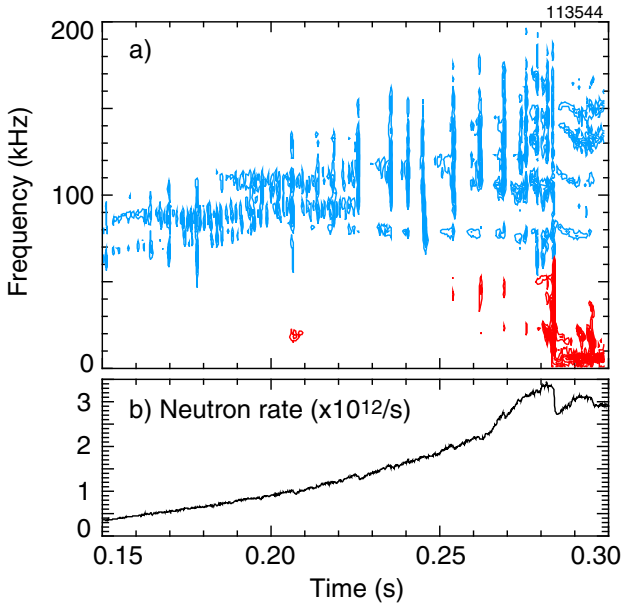

Figure 1. (*a*) The spectrogram of a Mirnov coil signal showing TAE behaviour in the frequency range between 60 and 200 kHz. (*b*) The neutron rate showing weak drops (<5%) at some TAE bursts.

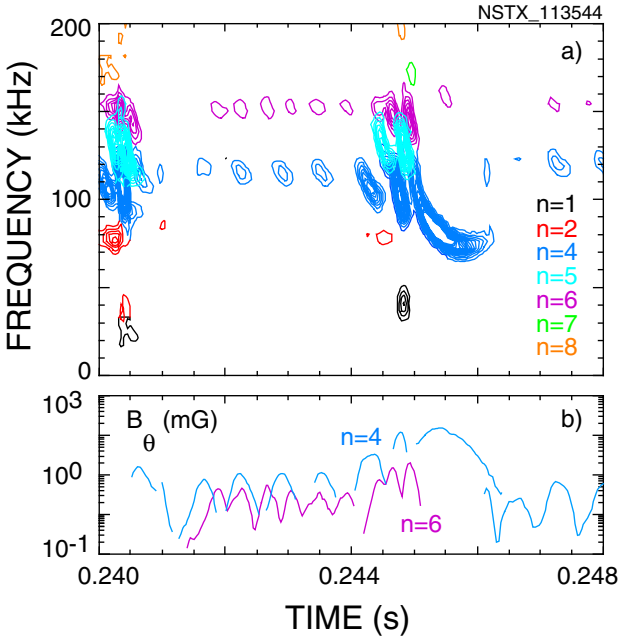

Figure 2. (*a*) The Mirnov coil spectrogram showing the TAE bursting cycle from 0.241 to 0.247 s, colours of contours indicate toroidal mode numbers, (*b*) amplitude of $n = 4$ magnetic fluctuations (blue) and $n = 6$ (magenta) found by tracking the mode in frequency versus time.

the reflectometers to measure mode amplitudes in the plasma core.

The electron temperature and density is measured at 17 ms intervals with a multi-channel Thomson scattering system [7]. The ion temperature and toroidal rotation are measured with a spectroscopic diagnostic looking at neutral beam charge-exchange-recombination light (CHERS) [8]. Measurement of the current profile with the motional stark effect (MSE) [9] diagnostic was not available at this time. The equilibrium flux surface geometry is constructed from external measurements of the magnetic field structure using the EFIT equilibrium code [10, 11]. The data on equilibrium parameters is integrated in the TRANSP code [12], which then calculates the neutral beam deposition profiles and fast ion slowing down distributions.

NSTX discharges heated by neutral beams typically exhibit a broad spectrum of fast ion driven instabilities. The spectrum shown in figure 1 shows bursting and chirping MHD activity (in blue) in the frequency range between 60 and 200 kHz. The bursting and chirping modes are in the frequency range expected for TAE. At lower frequencies (in red), e.g at 0.283 s in figure 1, are strongly chirping modes that have previously been identified as a form of energetic particle mode (EPM) [13–15]. They are localized in the plasma core and at the end of the frequency chirp, the mode frequency is nearly zero in the plasma frame. This paper will address the behaviour of the 60 to 200 kHz modes.

The modes in the TAE frequency range typically manifest as bursting, chirping modes, even at low amplitude (presumably with weaker drive). The saturated, coherent TAE seen on conventional aspect ratio tokamaks, excited by 2nd harmonic H-minority ion-cyclotron range of frequency (ICRF) heating [16–19] and sometimes with neutral beam heating (e.g. [20], figure 6), have not yet been seen in NSTX. The short bursts with small frequency chirps are in some cases interspersed with bursts that last longer and chirp over a wider frequency range (cf, figures 5 and 7, [15]), and are sometimes correlated with drops in the global neutron rate. These events more closely resemble the early observations of TAE excited by neutral beam heating in conventional tokamaks [21, 22]. Bursting–chirping modes, identified as TAE, have also been observed on START [23, 24] and MAST [25–27]. However, the range of the frequency chirps seen on MAST or START is often much larger than the range of the frequency chirping of the small bursts reported here.

The duration of each small burst is short, typically less than 0.5 ms, and the range of the frequency chirps is small, typically less than 10 to 15 kHz. The burst period ranges from ≈0.4 ms to ≈0.65 ms. The bursts appear in figure 1 as short, nearly vertical line segments and are better resolved in, for example, figure 2. In this shot, the sequences of weak bursts are punctuated by strong bursts with a period of 6 to 10 ms. Following each strong burst, there is a period of weaker mode activity.

Some of the strong bursts, but not all, are correlated with drops in the neutron rate, indicating losses of fast ions. Some of the drop in neutron rate could occur from redistribution of fast ions within the plasma, but the drops are also accompanied, in this case and others, by spikes in edge D-alpha light consistent with fast ions being lost. Also, for some shots, fast ion losses are measured directly [28]. In figure 3 is shown the correlation of mode activity with the neutron rate. In figure 3(*a*) are shown the edge magnetic fluctuation level (blue) and the core fluctuation level as measured with the reflectometer integrated over the frequency range 60–200 kHz, which in figure 1 is seen to cover the range of frequencies of the chirping mode activity. In figure 3(*b* is shown the time dependence of the neutron rate, and in figure 3(*c*) is shown the magnetic fluctuation level in the frequency range 10–60 kHz, corresponding to the frequency range of the EPMs seen in figure 1.

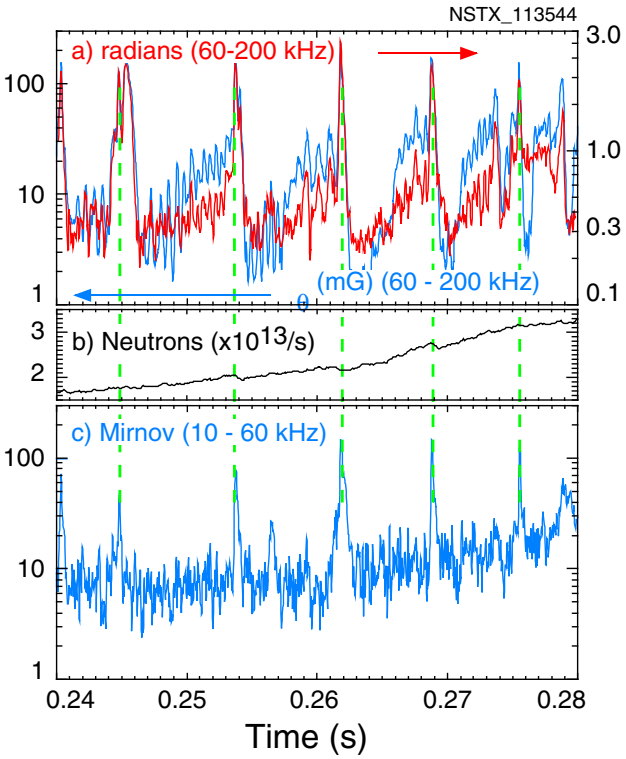

Figure 3. (*a*) rms fluctuation level integrated over the frequency band 60 to 200 kHz for a Mirnov coil (blue, mG) and for the 42 GHz quadrature reflectometer signal (red, radians), (*b*) neutron rate over this time interval, vertical green lines indicate strong TAE bursts, (*c*) fluctuation level from a Mirnov coil over the frequency range 10–60 kHz, the frequency band of EPMs.

In figure 3(*a*) it can be seen that the fluctuation amplitude goes through a cycle of slow growth in the peak amplitude of the bursts, culminating in a strong burst of activity lasting ≈1 msec. The mode amplitude drops to a low level following each large burst, and in some cases there is also a small drop in the neutron rate during the strong burst. Two representative examples of these cycles will be examined in greater detail. The cycle between roughly 0.241 and 0.247 s will be examined first and then the cycle between 0.262 and 0.269 s. There was no detectable drop in the neutron rate coincident with the strong burst at the end of the first of these two cycles. It was also different in that the period of high amplitude mode activity was longer, lasting roughly 2 msec.

In the spectrogram shown in figure 2, following the strong burst ending at 0.241 s, there is a sequence of five weak bursts at ≈120 kHz with toroidal mode number $n = 4$ (blue). The period of the bursts is about ≈0.65 ms and the weak frequency chirping is seen most clearly in the latter bursts. At about 150 kHz is seen a similar sequence of $n = 6$ bursts (magenta). The bursts are not synchronized with the $n = 4$ bursts and the period is slightly shorter, ≈0.5 ms.

The spectrogram of the Mirnov coil signal is constructed by overlaying spectrograms of the even and odd n toroidal fluctuations, allowing better discrimination of the modes. The multiple Fourier transforms are windowed with a Gaussian and overlapped to present a smoother evolution in time. In the spectrogram the contours are coloured to indicate the toroidal mode number.

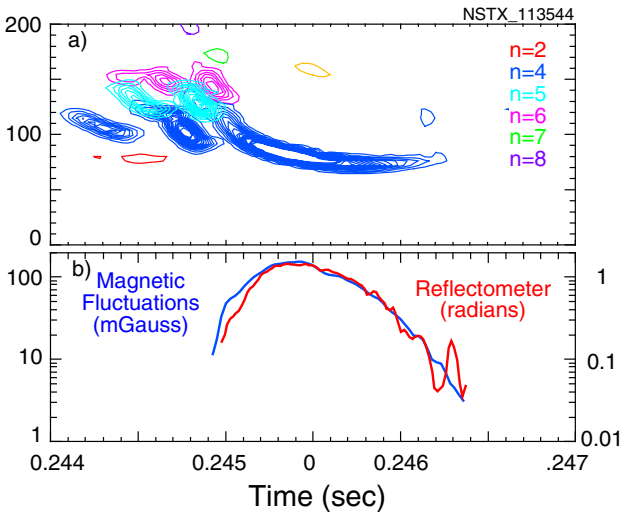

Figure 4. (*a*) The expanded spectrogram from figure 3 showing details of mode structure, (*b*) the amplitude of extended chirping mode in mG at wall (blue) and displacement in radians (red).

The initial growth rate $\gamma(=\gamma_L - \gamma_D)$ of the weak bursts (figure 2(*b*)) is $\gamma \approx 1.5 \times 10^4\ s^{-1}$. The decay rate of the bursts is also of the same order. If it is assumed that the mode drive is much reduced during the burst decay, $\gamma_L \approx 0$, then the burst growth and decay is consistent with $\gamma_L \approx 3 \times 10^4\ s^{-1}$ and $\gamma_D \approx 1.5 \times 10^4\ s^{-1}$.

In figure 2(*b*) is shown the amplitude evolution of the $n = 4$ (blue) and $n = 5$ (magenta) bursts. While the $n = 6$ burst peak amplitude is similar for the six bursts preceding the final large burst, the peak amplitude of the $n = 4$ bursts increases slowly during the cycle. Beginning at about 0.244 s the mode activity rapidly becomes more intense, with stronger $n = 4$ and $n = 6$ modes as well as the onset of strong $n = 5$ (cyan) and weak $n = 2$, 7 and 8 modes (red, green and orange, respectively).

The final strong burst of the cycle is shown in greater detail in figure 4. In figure 4(*a*) is an expanded spectrogram showing the sequence of $n = 4$, $n = 5$ and $n = 6$ bursts. There are two cycles consisting of an $n = 4$ burst, leading to an $n = 5$ and then $n = 6$ bursts with the final $n = 4$ burst having an extended frequency chirp phase lasting approximately 1.5 ms. The rate of the frequency chirp drops after the mode amplitude peaks. In figure 4(*b*) the Mirnov fluctuation amplitude evolution is compared with the internal mode amplitude evolution as measured with the 42 GHz reflectometer measuring mode amplitude at a major radius of 1.32 m (at $r/a \approx 0.5$). The evolution of the amplitudes tracks very well, which suggests that the radial structure of the mode is not changing significantly during the course of the chirp.

The second cycle ends at 0.2688 s, coincident with an approximately 5% drop in the neutron rate. The neutron rate is higher at the time of the second burst, suggesting a higher fast ion beta. Rather than the two modes ($n = 4$ and 6) present in the earlier cycle, here repetitive bursts of $n = 2$ through $n = 6$ modes are seen (figure 5, 0.266 to 0.2685 s). Unlike the earlier cycle, the timing of the different mode bursts seems to be correlated for the last three weak bursts preceding the strong burst. The amplitude of the bursts is less constant and the period of the bursts is shorter, ≈0.4 ms. The final

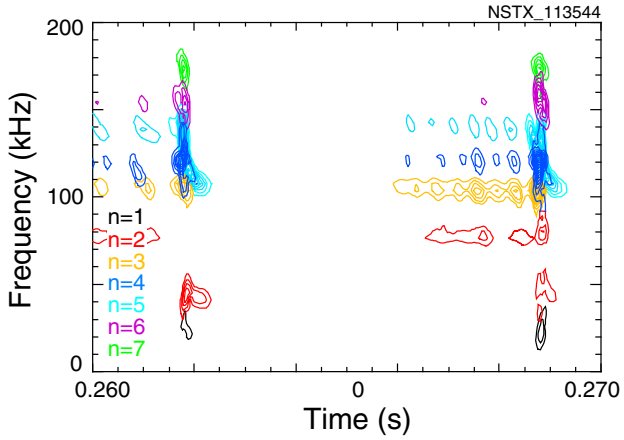

Figure 5. The spectrogram of magnetic fluctuations showing TAE cycle between 0.262 and 0.269 s. The colours of contours indicate toroidal mode numbers.

strong burst is shorter and consists simultaneously of modes with $n = 2$ through 7. The final burst lasts only ≈0.5 ms, making measurement of the growth rate of the individual modes difficult.

3. Analysis

The TRANSP code is used to map the diagnostic data, calculate the beam ion deposition profiles and slowing down distribution and to calculate the plasma rotation from the CHERS measurement of the impurity rotation profile. In figure 6 are shown the reflectometer measurements at 0.2688 s of the amplitude for the $n = 4$ mode at 117.2 kHz. The data (blue dots in figure 6(*a*)) suggest that the mode amplitude peaks between a major radius of roughly 1.3 and 1.4 m. In the same figure are shown profiles of additional parameters relevant to TAE instabilities. The fast ion β (figure 6(*a*), red curve) profile is strongly peaked but still retains significant amplitude in this radial range.

The $n = 3$ through $n = 5$ spectral peaks in figure 5 at this time have an average frequency separation of about 15 kHz. The frequencies of the individual modes are then nearly the same in the plasma frame. The Doppler shift inferred from the plasma rotation varies from ≈20 to ≈10 kHz in the radial range between 1.3 and 1.4 m, roughly consistent with the 15 kHz which would explain the observed separations. Some of this frequency shift might also come from the differences in the structure of the modes themselves. This is suggested by the larger frequency separation (≈25 kHz) between the $n = 2$ (red) and $n = 3$ (green) modes. A mode frequency nearly independent of the toroidal mode number is a characteristic of the TAE.

The initial velocity of full-energy neutral beam ions, even at 65 kV, is still more than twice the Alfvén velocity over most of the plasma. A profile of the ratio of beam ion birth velocity to local Alfvén speed is shown in figure 6(*b*) (blue curve). Towards the plasma edge, the ratio approaches two, thus beam ions with approximately one fourth the full energy can still be resonant with the TAE. The beam ion slowing down distribution around the outboard half-radius is shown in figure 7. As is typically the case in NSTX, the fast ion velocities

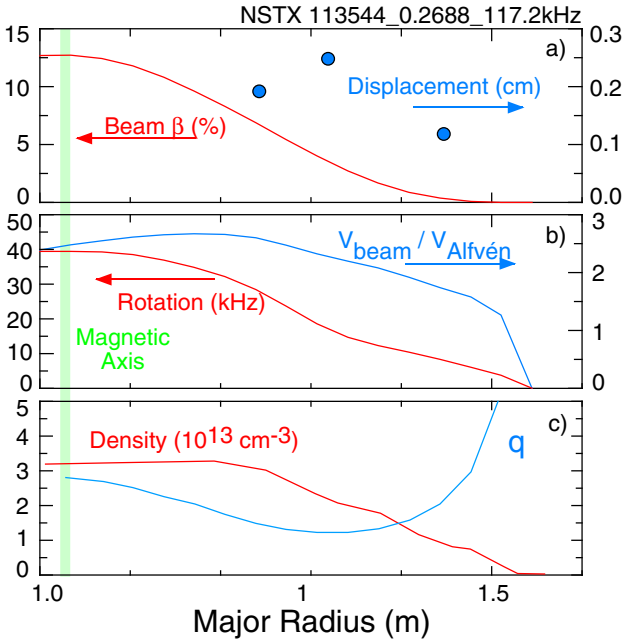

Figure 6. (*a*) The radial profile of fast ion beta at 0.27 s as calculated with TRANSP (red) and TAE mode amplitude as measured with the three quadrature reflectometer channels (blue dots), (*b*) the plasma toroidal rotation profile in kilohertz (red) and the ratio of the full energy beam speed to the Alfvén speed (blue), (*c*) the electron density profile (red) and q profile inferred by EFIT (blue).

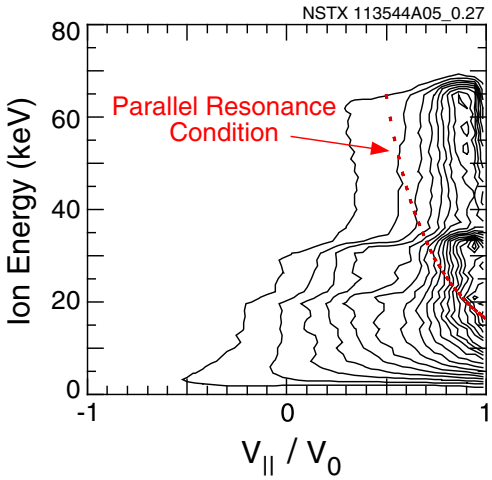

Figure 7. Fast ion distribution function as calculated by TRANSP at 0.27 s for approximately the half-radius on the outer midplane. The red curve indicates fast ions whose parallel velocity matches the Alfvén speed.

are predominantly parallel. The red curve indicates the parallel resonance condition that $V_{\text{Alfvén}} = V_{\text{Beam}}$. Ions above and to the right of the curve will be moving faster than the wave and can potentially contribute to instability. It should be noted that excitation of TAE has been observed on conventional aspect ratio tokamaks with $V_{\text{Alfvén}} \approx 0.7 V_{\text{Beam}}$ [21], so fast ions even below and to the left of this curve could potentially contribute. Of course the TRANSP calculation of the fast ion distribution does not include the possible effects of MHD instabilities on fast ion transport.

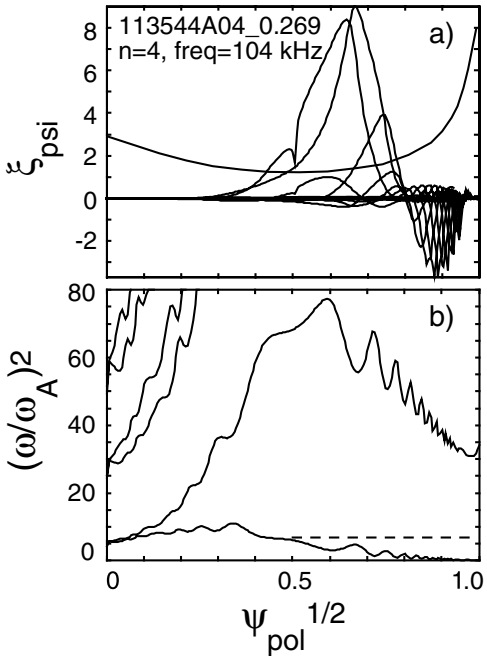

Figure 8. Eigenfunction of and gap structure for an $n = 4$ mode as calculated by NOVA-k for the parameters shown in figure 6. (*a*) The poloidal harmonics of the eigenfunction showing that the mode peaks near the minimum in the q profile (- - - -), (*b*) the calculated gap structure where the frequency is normalized with the NOVA formalism, $\omega_0 = V_{\text{Alfvén}}(0)/(q(a)R)$, $q(a) = 8.97$.

Modes in this frequency range and of this type in NSTX have been classified as TAE in previous works [28–33]. Simulations with the NOVA-k [34] code were used to support the identification of the modes as TAE. However, the q profile has not been directly measured but inferred with the equilibrium code EFIT and there is substantial uncertainty in the q profile shape, and thus the gap structure, eigenfrequencies and eigenmode shape. Such simulations are still useful in that they provide reasonable estimates of what the expected frequencies should be, as well as a guide as to what conditions might be expected to yield unstable modes.

The results of one such simulation with NOVA-k are shown in figure 8. The electron density and q profiles used in the simulation are those shown in figure 6(*c*). The current profile was not measured in this shot but calculated and inferred, with and without the measured kinetic pressure profile shape, with the EFIT equilibrium code. The $q(0)$ from these various estimates ranges from about 1.2 to 2.9 The uncertainty in the q-profile precludes anything more than a qualitative analysis of this data.

The gap is not open to the core (figure 8(*b*)) and the mode is localized to the outer region of the plasma with the amplitude peak just outside the location of the minimum in the q-profile, roughly consistent with the data shown in figure 6. While the mode interacts with the continuum, the continuum damping is still calculated to be much less than the drive. The predicted mode frequency is 104 kHz and the damping and growth rates as normalized to the mode frequency, γ_j/ω, are given in table 1. The net calculated growth rate, normalized to the mode frequency, is then about 3%, with the drive approximately ten times higher than the net damping.

Table 1.

Continuum	−0.003%
Electron collisional	−0.100%
Electron Landau	−0.027%
Ion Landau	−0.200%
Beam, FLR + FOW	3.200%

The ability to measure the internal amplitude of the mode provides valuable, quantitative information about the non-linear growth and saturation physics. The quadrature reflectometers measure the displacement of the cut-off density layer, i.e. an internal point measurement of the mode amplitude. For the modes in the strong burst, the peak displacement is about 0.25 cm or $\delta n/n \approx 1\%$. The weaker bursts are about a factor of ten smaller than this. This measurement can be related, through a calculation of the linear eigenmode, to the local electric field fluctuation amplitude and from there to the wave-trapped fast ion bounce frequency. Using NOVA to relate the density fluctuation amplitude to the wave-trapped fast ion bounce frequency for the eigenfunction shown in figure 8, the mode amplitude, expressed in terms of the bounce frequency, is $\approx 3.4 \times 10^4\,\text{rad}\,\text{s}^{-1}$ for a density fluctuation level of 0.1%.

NOVA predicts significant reduction of the bounce frequency due to finite beam ion orbit and Larmor radius effects due to weaker interaction with the mode, since $k_\wedge r \gg 1$ for moderate n number TAEs in NSTX. NOVA evaluates the expression for the effective collisional frequency, ν_{eff}:

$$\nu_{\text{eff}}^3 = \nu_c < |\partial P_\phi/\partial(\boldsymbol{v}/v)|^2 > (\partial\Omega/\partial P_\phi|_{H'})^2,$$

where ν_c is the 90° pitch-angle scattering rate, Ω is the resonance condition and P_ϕ and H are the particle canonical momentum and energy [35, 36]. The calculation in NOVA averages over the phase space of fast ions, weighted by the resonant drive to the mode. For the considered case we find that $\nu_{\text{eff}} = 1.8 \times 10^4\,\text{s}^{-1}$.

4. Discussion

A definitive identification and study of the modes shown here will require measurement of the current profile which was not available at this time. However, it is possible at this point to make some qualitative interpretations of the observed modes and their behaviour. Comparison of the observed mode frequencies and toroidal mode numbers to the NOVA-k and M3D simulations suggests identification of these modes as TAE-like instabilities. Both the weak and strong bursting behaviour has been predicted for regimes of fast ion driven instabilities. Strongly chirping modes in this frequency range have also been observed on MAST and been identified as TAE [25,26] and the frequency chirping attributed to 'hole-clump'-like behaviour [27]. Weak chirping and bursting TAE have been simulated with M3D for similar NSTX parameters [33]. In these simulations the frequency chirping was, at least in part, ascribed to a change in the mode structure during the burst.

The qualitative non-linear behaviour of fast ion driven instabilities depends on the relative size of several parameters

[37]. These include the linear drive for the mode, γ_L, the sum of the mode damping terms, γ_D, the wave-trapped fast ion bounce frequency, ω_b, as defined above and the effective fast ion distribution relaxation rate, ν_{eff}. The relaxation rate is a measure of the timescale over which a perturbation to the distribution function caused by a transient mode will relax towards its undisturbed state.

It has been shown that in the regime where $\nu_{eff} \geqslant \gamma_D$ modes tend towards a steady-state saturation and in the opposite limit, $\gamma_D \gg \nu_{eff}$ modes will have a bursting character [37]. The observed modes exhibit bursting, albeit a complicated cycle, suggesting that this mode is in the latter regime. In the former ('steady-state') regime the mode amplitude will saturate at an amplitude where $\omega_b > \gamma_L$. In the bursting regime, the mode amplitude will peak at an amplitude where $\omega_b \approx \gamma_L$. The estimate of $\omega_b \approx 3.4 \times 10^4\,\mathrm{rad\,s^{-1}}$ in the previous section for the weakly bursting instabilities is reasonably close to the estimate of the linear growth rate $\gamma_L \approx 3 \times 10^4\,\mathrm{s^{-1}}$ found in section 2 and the growth rate predicted estimate from NOVA-k.

In numerical simulations of bursting modes [37] it has been found that the time interval between the pulses is of the order ν_{eff}^{-1}. The period of the weakly bursting modes (section 2) then yields $\nu_{eff} \approx 1.5\text{–}2.5 \times 10^3\,\mathrm{s^{-1}}$. Using the damping rate estimate from section 2 puts these modes in the regime where $\gamma_D \approx 1.5 \times 10^4\,\mathrm{s^{-1}} \gg \nu_{eff}$, i.e. the bursting regime. However, the NOVA-k estimate of $\nu_{eff} \approx 1.8 \times 10^4\,\mathrm{s^{-1}}$, for an unperturbed fast ion population, is larger than the empirical estimate and is comparable to the mode damping rate. Since the modes are clearly present in a non-equilibrium condition, it is possible that the equilibrium fast ion distribution function may not be a good estimate.

The transition from 'weak', uncorrelated $n = 4$ and $n = 6$ bursts to the strong, multi-mode bursts at the end of each cycle is suggestive of the 'avalanche' effect predicted when modes with nearby resonances in phase space reach sufficient amplitude so that the fast ion phase space trajectories begin to overlap [38–41]. In this case, the modes are able to access much more free energy from the fast ion distribution and are predicted to grow explosively, leading to a substantial modification of the fast ion distribution. The modification of the fast ion distribution may then excite modes which until then had been linearly stable, e.g. the $n = 5$ modes in figure 4. It is this type of physics which may play an important role in the TAE-induced fast ion transport in future large scale fusion devices such as ITER [42].

The strong frequency chirping seen for the $n = 4$ mode in figures 3 and 4 is suggestive of the hole-clump theory developed by Berk, Breizman and Petviashvilli [43–45]. Although only the downward chirping (clump) branch is seen, it is perhaps the case that the strong $n = 5$ and $n = 6$ modes interfered with the formation of the upward chirping (hole) branch.

With the diagnostic tools presently available on NSTX, it should be possible in the future to provide quantitative tests of these non-linear models for TAE growth, saturation and fast ion transport. However such calculations will need to wait until a measurement of the q profile is available, allowing a definitive calculation of the eigenmode structure for the fast ion driven instabilities. Further, the inclusion of additional physics effects in the NOVA-k modelling is being explored which may lead to refinements in the interpretation of these modes.

Acknowledgments

The authors are grateful for the support of the NSTX team of physicists and engineers. This work is supported by the U.S. DoE contract DE-AC02-76CH03073.

References

[1] ITER Physics Basis Editors *et al* 1999 *Nucl. Fusion* **39** 2137
[2] Cheng C.Z. and Chance M.S. 1986 *Phys. Fluids* **29** 2471
[3] Wong K.L. *et al* 1991 *Phys. Rev. Lett.* **66** 1874
[4] Heidbrink W.W., Strait E.J., Doyle E., Sager G. and Snider R.T. 1991 *Nucl. Fusion* **31** 1635
[5] Ono M. *et al* 2000 *Nucl. Fusion* **40** 557
[6] Kubota S., Nguyen X.V., Peebles W.A., Zeng L. and Doyle E.J. 2001 *Rev. Sci. Instrum.* **72** 348
[7] Johnson D.W., Bretz N., LeBlanc B., Palladino R., Long D. and Parsells R. 1999 *Rev. Sci. Instrum.* **70** p 776
[8] Bell R.E. *et al* 1996 *Proc. 23rd European Physical Society Conf. on Plasma Physics and Controlled Fusion Research (Kiev)* vol 20C Part I (Geneva: The European Physical Society 1996) p 59
[9] Levinton F.M. and Zarnstorff M.C. 1995 *Phys. Rev. Lett.* **75** 4417
[10] Lao L.L., St John H., Stambaugh R.D., Kellman A.G. and Pfeiffer W.P. 1985 *Nucl. Fusion* **25** 1611
[11] Sabbagh S.A. *et al* 2001 *Nucl. Fusion* **41** 1601
[12] Budny R.V. 1994 *Nucl. Fusion* **34** 1247
[13] Fredrickson E.D., Chen L. and White R.B. 2003 *Nucl. Fusion* **43** 1258
[14] Kolesnichenko Ya.I., Marchenko V.S. and White R.B. 2006 *Phys. Plasmas* **13** 052504
[15] Fredrickson E.D. *et al* 2006 *Phys. Plasmas* **13** 056109
[16] Wong K.L., Wilson J.R., Chang Z.Y., Fu G.Y., Fredrickson E., Hammett G.W., Bush C., Phillips C.K., Snipes J. and Taylor G. 1994 *Plasma Phys. Control. Fusion* **36** 879
[17] Fasoli A. *et al* 1997 *Plasma Phys. Control. Fusion* **39** B 287
[18] Saigusa M., Kimura H., Kusama Y., Kramer G.J., Ozeki T., Moriyama S., Oikawa T., Neyetani Y. and Kondoh T. 1998 *Plasma Phys. Control. Fusion* **40** 1647
[19] Heidbrink W.W., Fredrickson E.D., Mau T.K., Petty C.C., Pinsker R.I., Porkolab R.I. and Rice B.W. 1999 *Nucl. Fusion* **39** 1369
[20] Strait E.J., Heidbrink W.W. and Turnbull A.D. 1994 *Plasma Phys. Control. Fusion* **36** 1211
[21] Wong K.L. *et al* 1992 *Phys. Fluids* B **4** 2122
[22] Heidbrink W.W., Duong H.H., Manson J., Wilfrid E. and Oberman C. 1993 *Phys. Fluids* B **5** 2176
[23] McClements K.G., Gryaznevich M.P., Sharapov S.E., Akers R.J., Appel L.C., Counsel G.F., Roach C.M. and Majeski R. 1999 *Plasma Phys. Control. Fusion* **41** 661
[24] Gryaznevich M.P. and Sharapov S.E. 2000 *Nucl. Fusion* **40** 907
[25] Gryaznevich M.P. and Sharapov S.E. 2004 *Plasma Phys. Control. Fusion* **46** s15
[26] Pinches S.D., Berk H.L., Grayaznevich M.P., Sharapov S.E. and JET-EFDA Contributors 2004 *Plasma Phys. Control. Fusion* **46** S47
[27] Sharapov S.E. *et al* and JET-EFDA Contributors and the Mast Team 2005 *Nucl. Fusion* **45** 1168–77
[28] Fredrickson E.D. *et al* 2003 *Phys. Plasmas* **10** 2852
[29] Gorelenkov N.N., Cheng C.Z., Fu G.Y., Kaye S., White R. and Gorelenkova M.V. 2000 *Phys. Plasmas* **7** 1433
[30] Heidbrink W.W., Fredrickson E., Gorelenkov N.N., Hyatt A.W., Kramer G. and Luo Y. 2003 *Plasma Phys. Control. Fusion* **45** 983

[31] Fredrickson E.D. *et al* 2004 *Proc. 20th Int. Conf. on Plasma Physics and Controlled Nuclear Fusion Research (Vilamoura, Portugal)* Paper IAEA-EX/5-3
[32] Gorelenkov N.N., Belova E.V., Berk H.L., Cheng C.Z., Fredrickson E., Heidbrink W.W., Kaye S. and Kramer G.J. 2004 *Phys. Plasmas* **11** 2586
[33] Fu G.Y., Breslau J., Fredrickson E., Park W. and Strauss H.R. 2004 *Proc. 20th Int. Conf. on Plasma Physics and Controlled Nuclear Fusion Research (Vilamoura, Portugal)* Paper IAEA-TH/P4-38
[34] Cheng C.Z. 1992 *Phys. Rep.* **211** 1–51
[35] Berk H.L., Breizman B.N. and Pekker M. 1997 *Plasma Phys. Rep.* **23** 778
[36] Gorelenkov N.N., Chen Y., White R.B. and Berk H.L. 1999 *Phys. Plasmas* **6** 629
[37] Berk H.L., Breizman B.N. and Pekker M. 1995 *Phys. Plasmas* **2** 3007
[38] Berk H.L., Breizman B.N. and Ye H. 1992 *Phys. Lett.* A **162** 475
[39] Berk H.L., Breizman B.N., Fitzpatrick J. and Wong H.V. 1995 *Nucl. Fusion* **35** 1661
[40] Berk H.L., Breizman B.N. and Pekker M. 1995 *Nucl. Fusion* **35** 1713
[41] Berk H.L., Breizman B.N. and Pekker M. 1996 *Phys. Rev. Lett.* **76** 1256
[42] Gorelenkov N.N., Berk H.L. and Budny R.V. 2005 *Nucl. Fusion* **45** 226–37
[43] Berk H.L., Breizman B.N. and Petviashvili N.V. 1997 *Phys. Lett.* A **234** 213
[44] Berk H.L., Breizman B.N., Candy J., Pekker M. and Petviashvili N.V. 1999 *Phys. Plasmas* **6** 3102
[45] Vann R.G.L., Dendy R.O. and Gryaznevich M.P. 2005 *Phys. Plasmas* **12** 032501